Çukurova Üniversitesi
Mühendislik Fakültesi Dergisi
Çukurova University
Journal of the Faculty of Engineering
ISSN: 2757-9255 CİLT/VOLUME: 40 SAYI/ISSUE: 2 HAZİRAN/JUNE 2025

Progressive Collapse and Robustness Analysis of Steel Structures

Jülide YÜZBAŞI [1,a]

[1]*Cukurova University, Engineering Faculty, Department of Civil Engineering, Adana, Türkiye*

[a]***ORCID**: 0000-0002-4034-5666*

Article Info
Received : 07.05.2025
Accepted : 16.06.2025
DOI: 10.21605/cukurovaumfd.1694613

Corresponding Author
Jülide YUZBASI
jyuzbasi@cu.edu.tr

Keywords
Steel structures
Progressive collapse (PC)
Earthquakes
Nonlinear dynamic analysis (NDA)
Solid mechanics

***How to cite:** YÜZBAŞI, J., (2025). Progressive Collapse and Robustness Analysis of Steel Structures. Cukurova University, Journal of the Faculty of Engineering, 40(2), 429-444.*

ABSTRACT

This study investigates the progressive collapse behavior of a five-story, three-dimensional steel moment-resisting frame using the Applied Element Method (AEM). The model represents an existing multi-story full-scale steel structure located in the United States once, incorporating realistic geometric and structural characteristics. The structural system comprises rigid beam-to-column connections, ensuring full moment transfer across joints. The frame geometry includes seven spans in the longitudinal direction and three spans in the transverse direction, with non-uniform bay widths and varying story heights, reflecting a realistic high-rise configuration. Three critical column removal scenarios were modeled: (1) the middle of the short side, (2) the middle of the long side, and (3) a corner column at the first story. AEM was adopted to simulate highly nonlinear phenomena. Removing the middle column on the long side resulted in the highest displacements, underscoring the critical influence of column location on progressive collapse vulnerability and robustness.

Çelik Yapıların İlerlemeli-Aşamalı Göçme ve Dayanıklılık Analizi

Makale Bilgileri
Geliş : 07.05.2025
Kabul : 16.06.2025
DOI: 10.21605/cukurovaumfd.1694613

Sorumlu Yazar
Jülide YUZBASI
jyuzbasi@cu.edu.tr

Anahtar Kelimeler
Çelik yapılar
İlerlemeli-aşamalı göçme
Depremler
Doğrusal olmayan dinamik analiz
Katı cisimler mekaniği

***Atıf şekli:** YÜZBAŞI, J., (2025). Farklı Çelik Yapıların İlerlemeli-Aşamalı Göçme ve Dayanıklılık Analizi. Çukurova Üniversitesi, Mühendislik Fakültesi Dergisi, 40(2), 429-444.*

ÖZ

Bu çalışma, Uygulamalı Elemanlar Yöntemi (AEM) kullanılarak beş katlı, üç boyutlu bir çelik moment taşıyıcı çerçevenin ilerlemeli göçme davranışını incelemektedir. Model, geçmişte ABD'de bulunan mevcut çok katlı bir çelik yapıyı, gerçekçi geometrik ve yapısal özellikleriyle temsil etmektedir. Yapısal sistem, rijit kiriş-kolon birleşimleriyle tam moment aktarımı sağlayan bağlantılardan oluşmaktadır. Taşıyıcı sistemin geometrisi, boyuna yönde yedi, enine yönde üç açıklıktan oluşmakta olup, açıklık genişlikleri düzensiz ve kat yükseklikleri değişkendir—bu durum, gerçekçi bir yüksek yapı düzenini yansıtmaktadır. Üç kritik kolon kaybı senaryosu modellenmiştir: (1) kısa kenarın ortası, (2) uzun kenarın ortası ve (3) birinci kattaki köşe kolonu. AEM, yüksek derecede doğrusal olmayan davranışları simüle etmek için kullanılmıştır. Uzun kenarın ortasındaki kolonun kaldırılması en büyük yer değiştirmelere yol açmıştır. Bu durum kolon konumunun ilerleyici göçme hassasiyeti ve yapısal dayanıklılık üzerindeki belirleyici etkisini ortaya koymuştur.

1. INTRODUCTION

Progressive collapse refers to a phenomenon in which local damage triggers a chain reaction of structural failures, ultimately resulting in partial or complete collapse of a building or infrastructure. This type of collapse can be initiated by various extreme events, including explosions, fire, seismic activity, and design or construction deficiencies—each revealing how vulnerable even modern structures can be when robustness is not adequately ensured. Unlike standard performance analyses, progressive collapse analysis aims to ensure that the building does not experience total collapse when any column is removed. To achieve this, the analysis focuses on identifying weaker points in the structure, which can then be strengthened by detecting critical locations.

Although progressive collapse was once considered a rare occurrence, a series of dramatic failures over the past several decades—ranging from the Ronan Point disaster in 1968 to more recent collapses caused by earthquakes, terrorist attacks, and structural inadequacies—has demonstrated that the risks are both systemic and globally distributed [1,2]. Consequently, the phenomenon has drawn increasing attention in recent decades, particularly as real-world disasters continue to expose critical weaknesses in structural systems. Table 1 provides a chronological overview of such notable events, emphasizing the wide range of initiating causes as well as the geographic and structural diversity of affected buildings.

Table 1. Notable instances of progressive collapse due to extreme events

Event	Location	Year	Cause/Trigger
Ronan Point	London, UK	1968	Gas explosion
Capitan Arenas Collapse	Barcelona, Spain	1972	Unknown
U.S. Marine Barracks Attack	Beirut, Lebanon	1983	Bomb attack
Hotel New World Collapse	Singapore	1986	Unknown
A.P. Murrah Federal Building	Oklahoma, USA	1995	Bomb attack
Sampoong Department Store	Seoul, South Korea	1995	Structural failure
Khobar Towers	Saudi Arabia	1996	Attack
World Trade Center	New York City, USA	2001	Attack (9/11)
Windsor Tower Fire	Madrid, Spain	2005	Fire
Achimoto Melcom Shopping Centre	Accra, Ghana	2012	Structural failure
Rana Plaza Factory	Dhaka, Bangladesh	2013	Structural failure
Morandi Bridge Collapse	Genoa, Italy	2018	Structural failure
Kubilay and Mete Buildings	Turkiye	2023	Kahramanmaras Earthquake (7.8 & 7.6 magnitude)
Steel Demir Building	Antakya, Turkiye	2023	Kahramanmaras Earthquake (7.8 & 7.6 magnitude)
High-rise Building Collapse (Under construction)	Chatuchak, Bangkok	2025	Myanmar Earthquake (7.7 magnitude)

Despite the growing body of research on progressive collapse, a significant portion of the existing literature has historically centered around reinforced concrete structures, leaving steel-framed systems comparatively less examined [3-8]. While steel structures are often perceived as inherently robust due to their ductility and redundancy, recent real-world failures have challenged this assumption and revealed critical knowledge gaps in how such systems perform when subjected to localized damage combined with extreme scenarios.

Recent earthquake events, such as the 2023 Kahramanmaraş earthquakes, have highlighted various structural vulnerabilities across different building types. Commonly observed failures include soft and weak story mechanisms, insufficient material strength, inadequate detailing of reinforcement, poor workmanship, and liquefaction-induced foundation instabilities. These deficiencies have significantly contributed to structural collapses, underscoring the need for improved design and construction practices, even in steel structures, which were previously considered more resilient.

After the 2023 Kahramanmaraş earthquakes [9-11], a particularly revealing example was the progressive collapse of a steel building in Antakya, Türkiye. Occurring in a highly seismic region with aging infrastructure, this incident exposed unexpected weaknesses in the seismic resilience of steel structures and

emphasized the need to revisit design assumptions and detailing strategies. What sets the Antakya failure apart is that it occurred despite the expected seismic advantages of steel, such as superior energy absorption and deformation capacity (Figures 1–3). This failure makes clear that material properties alone cannot guarantee structural robustness. Instead, ensuring resilience against disproportionate collapse requires an integrated approach that accounts for load redistribution mechanisms, connection detailing, and the compound effects of multiple hazards. The following figures chronologically depict the structure's condition before the event (Figure 1), the visible external damage immediately afterward (Figure 2), and the critical failure zones identified at the beam-column connections (Figure 3).

Figure 1. Undamaged condition of the steel-framed building in Antakya, Türkiye, before the earthquakes

Figure 2. Post-earthquake exterior view of the same steel building

Figure 3. Buckled steel column and close-up of localized damage at beam-column connections

Such recent events highlight that steel-framed systems also warrant careful assessment, especially if they consist of multi-story. As such, this case serves not only as a critical example of unforeseen vulnerability but also as the primary motivation for the present study. Several studies have addressed different strategies to enhance the progressive collapse resistance of steel-framed structures. Alashker et al. [12] investigated the effectiveness of fiber-reinforced polymers (FRP) in strengthening steel moment frames against progressive collapse. Bao and Yang [13] focused on the energy flow mechanisms during the collapse process to better understand how energy is redistributed and dissipated. Bregoli et al. [14] examined the robustness of modular steel-framed buildings by applying the alternative load path method, which helps identify potential vulnerabilities in structural systems. Similarly, Lu et al. [15] assessed the performance of high-rise steel moment frames designed for seismic resistance. Li et al. [16] assessed collapse fragility under mainshock–aftershock sequences, and Stochino et al. [17] focused on structural robustness and resilience under extreme loads. Additionally, Işık et al. [18] investigated the influence of vertical ground motions on steel structures across different seismic zones. These studies underscore the necessity for more refined computational modeling, scenario-based analysis, and performance-driven assessment methods.

Therefore, this study seeks to advance the growing body of research by examining the progressive collapse behavior and structural robustness of steel buildings subjected to various column removal scenarios. To this end, Section 2 provides a detailed overview of the progressive collapse allowances specified in the General Services Administration (GSA) and Unified Facilities Criteria (UFC) guidelines, followed by an introduction to the Applied Element Method (AEM), a relatively recent approach compared to the conventional Finite Element Method (FEM) [19-21]. Section 3 presents the main steel model, developed based on a real-world construction project, and outlines the column removal scenarios investigated in the study [22]. Section 4 discusses the analytical models and presents the maximum transient and residual displacements resulting from different column loss cases, supported by graphical representations to aid interpretation. Finally, Section 5 offers a synthesis of the key findings and conclusions drawn from the study.

2. METHOD

2.1. Overview of Progressive Collapse Allowances in GSA and UFC Guidelines

General Services Administration (GSA) defines ***progressive collapse*** as a sequential failure mechanism where an initial localized damage propagates from one structural component to another, potentially leading to the failure of a substantial portion or the entirety of the structure [23]. This definition aligns with that of ASCE 7-05, which characterizes progressive collapse as “the spread of an initial local failure from element to element resulting, eventually, in the collapse of an entire structure or a disproportionately large part of it.”

Furthermore, as noted in the *Review of International Research on Structural Robustness and Disproportionate Collapse by the Centre for the Protection of National Infrastructure (CPNI)*, progressive collapse refers specifically to the mechanism by which collapse develops—often described metaphorically as a "*domino effect*."

In contrast, *disproportionate collapse* refers to how large or severe the overall collapse is compared to the original cause. In this context, "disproportionate" highlights the mismatch between the scale of the initial damage and the resulting consequences. For example, a collapse can be progressive—spreading from one part to another—but not disproportionate if it stops after a few structural bays. On the other hand, a collapse can be disproportionate—causing major damage from a small initial failure—without being progressive, such as when a single large bay collapses entirely without affecting other parts of the structure.

The former guidelines focused specifically on *Collapse Prevention* performance criteria and modeling approaches for reinforced concrete and structural steel elements. According to ASCE 41 (Table C1-2 and Section C1.5.1.5), Collapse Prevention represents a condition in which the structure is on the verge of collapse but still manages to maintain its ability to support gravity loads [24].

At this performance level, the following can be expected:

- Overall structural damage is severe.
- There is very little remaining stiffness or strength, but key vertical load-carrying elements like columns and walls are still standing and functioning.

- The building is technically not safe to occupy and unlikely to be repairable in a cost-effective way.

In accordance with ASCE 41-17, Section 7.6.3 offers guidance for establishing modeling parameters and acceptance criteria for structural subassemblies based on experimental testing. It provides practical guidance on how to define modeling parameters and acceptance criteria for structural subassemblies using test results. Although the full standard is not included here, important points are highlighted where needed for clarity.

The experimental studies referenced showed that most components followed Type 1 or Type 2 backbone curves, meaning they responded in a ductile and deformation-controlled manner. However, a few very slender columns failed early due to global lateral-torsional buckling before reaching yield, which is a form of instability rather than typical inelastic behavior. Importantly, none of the specimens showed Type 3 behavior, which is associated with force-controlled and brittle failure.

For each specimen, a backbone curve was developed by tracing the envelope of the first cycle in the hysteresis loop. These curves were compared with the standardized force-deformation relationship shown in ASCE 41-17 Figure 9-1 (reproduced as Figure 4 here). Key points on the curve—labeled B, C, D, and E—were recorded to define performance levels.

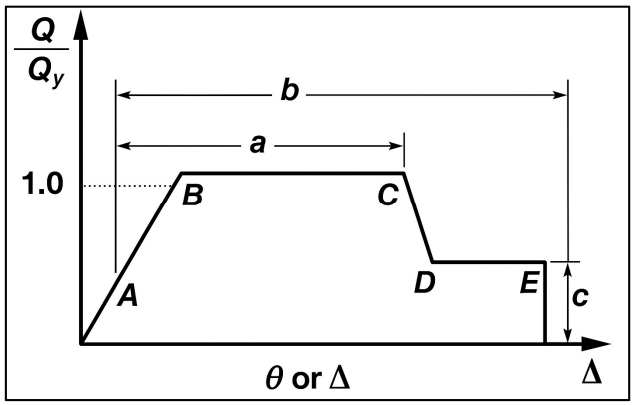

Figure 4. Backbone curve curve showing performance parameters based on ASCE 41-17

Section ASCE 41-17, Section 7.6.3 also explains how to determine nonlinear acceptance criteria based on test results:

- Immediate Occupancy (IO) is defined as 75% of the deformation at point C (maximum moment before degradation).
- Life Safety (LS) is defined as 75% of the deformation at point E (maximum deformation before collapse).
- Collapse Prevention (CP) is taken as the full deformation at point E.

The difference between point C and the yield point gives the “a” parameter listed in Table 9-6, while the difference between point E and the yield point gives the “b” parameter. The “c” parameter represents the ratio of strength at point E to the expected yield strength. In specimens with significant strain hardening, this ratio can be greater than 1.0. These a, b, and c values were obtained through regression analysis of the test data.

As a reminder, the force–displacement curve corresponding to these performance levels is also presented in Fig. 5, as specified in TBEC 2018.This curve is particularly significant because it underpins the evaluation of structural components at different performance levels, including the *Collapse Prevention*

performance level. Collapse Prevention represents the most critical performance objective, wherein the structure is expected to sustain severe deformations while still avoiding total collapse. Specifically, the *Collapse Prevention* performance level—considered the most critical threshold—focuses on ensuring that the structure maintains its ability to resist gravity loads despite severe deformations and significant damage. At this level, substantial structural degradation is permissible as long as total collapse is prevented, thereby prioritizing the preservation of life over reparability (Figure 5).

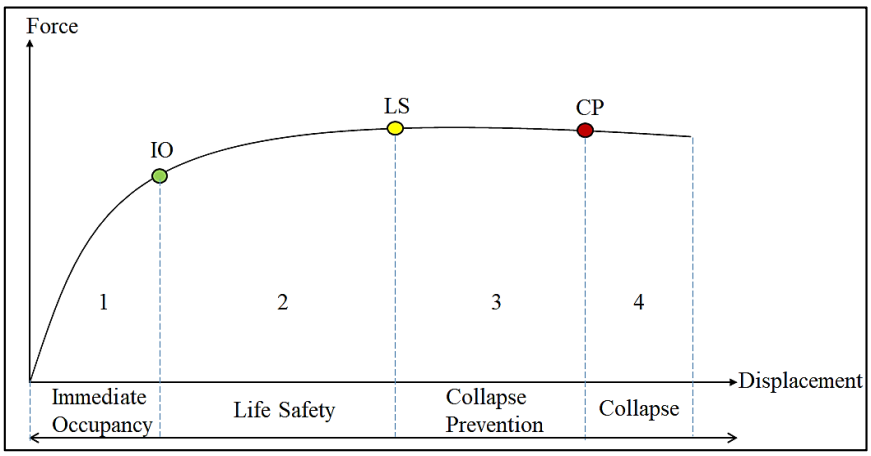

Figure 5. Force–Displacement curve ıllustrating performance levels based on TBEC 2018

It's important to clarify that the purpose of Collapse Prevention in the context of progressive collapse design is not to ensure that the building remains usable or easily repairable after an extreme event. Instead, the goal is to limit the spread of damage so that it does not result in a total or disproportionate collapse, and so that emergency evacuation can take place safely.

Given experimental evidence showing that reinforced concrete and steel elements can sustain large plastic deformations, the Collapse Prevention performance level is deemed both appropriate and pragmatic when designing against progressive collapse.

Earlier versions of the GSA Guidelines (e.g. 2003) permitted a limited extent of collapse following the removal of a vertical load-bearing element. Under these provisions, collapse was restricted to the structural bays directly connected to the removed element, and only at the floor level immediately above. Maximum allowable collapse areas were set at 1,800 ft² for exterior column removal and 3,600 ft² for interior column removal scenarios.

Similarly, ***earlier editions*** of the Unified Facilities Criteria (UFC) adopted an area-based definition for acceptable collapse. In these documents, collapse resulting from the removal of an exterior column was limited to 15% of the floor area directly above, whereas interior column removal permitted collapse up to 30% of the floor area at the same level.

In contrast, the current version of the ***UFC no longer permits any predefined or acceptable collapse area*** [25]. All structural components, including those located directly above the removed element, must be designed to meet specific acceptance criteria. This approach reflects a transition from collapse tolerance toward a stricter emphasis on structural robustness and integrity, aiming to ensure that no portion of the structure undergoes collapse under the prescribed removal scenarios.

Moreover; in the 2016 revision of the General Services Administration (GSA, 2016) guidelines, ***a significant shift was introduced*** in the criteria used to determine the applicability of progressive collapse analysis requirements. Unlike the earlier 2003 version, which relied primarily on building height as a determinant, the updated guidelines adopt a risk-based approach by incorporating the *Facility Security Level (FSL)*. The FSL classification considers factors such as mission criticality, facility size, tenant population, and potential threats to determine the required level of structural robustness. This revision aimed to align the GSA's progressive collapse mitigation strategies with the Interagency Security Committee (ISC) Risk Management Process and reduce misapplications stemming from height-based

thresholds. As a result, the 2016 guidelines promote a more consistent and threat-responsive design framework, particularly for government facilities with heightened security concerns.

The Facility Security Level (FSL) is a risk-based classification system introduced in the 2016 revision of the GSA (GSA, 2016) progressive collapse guidelines to better tailor security requirements to individual facilities. The FSL is determined through a structured evaluation of five factors: mission criticality, symbolism, facility population, facility size, and threat level. Each factor is assigned a numerical score, and the cumulative result places the building into one of five FSL categories (I through V), ranging from lowest to highest risk. Higher FSL levels imply a greater need for robustness in structural design due to increased threat or operational importance.

Table 2. Summary of Facility Security Level (FSL) classification criteria

Factor	Description	Scoring (Indicative)
Mission Criticality	Importance of the facility's operations to national or agency missions	Low to High (1–5)
Symbolism	Degree to which the facility represents a national or political symbol	Low to High (1–5)
Population	Number of regular occupants in the facility	<10 to >450 (1–5)
Facility Size	Total area of the building or complex	Small to Large (1–5)
Threat Level	Intelligence-based assessment of potential threats	Minimal to Severe (1–5)

Final FSL Level (I–V) is determined by the cumulative score and professional judgment in accordance with ISC standards.

In accordance with the General Services Administration (GSA) 2016 guidelines, a systematic approach must be adopted for column removal to evaluate the progressive collapse resistance of a structure. For *internal columns*, particularly in areas with underground parking or regions with uncontrolled public access, removal scenarios are conducted at the midpoints of the short and long spans and at the corners of the uncontrolled areas. These removals are performed over a single story, extending from the parking or public-access level to the level immediately above. Similar to the external removal protocol, additional internal column removals are mandated at critical structural irregularities, again applying the 30% proximity criterion to account for nearby column interactions. This comprehensive strategy ensures a robust assessment of a building's vulnerability to progressive collapse under abnormal loading conditions (Figure 6).

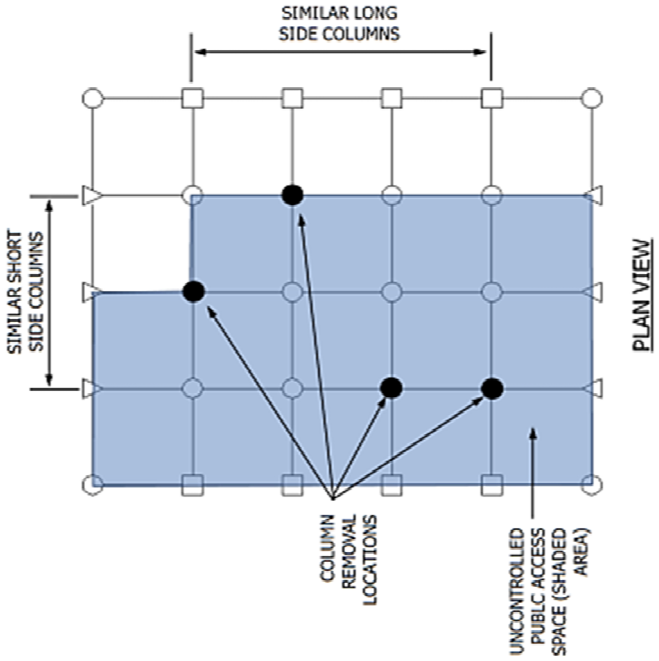

Figure 6. Location of internal column removal (GSA, 2016)

For *external columns*, removals should be conducted at multiple strategic locations, including the midpoints of both short and long facades, the corners, and the penultimate (adjacent-to-corner) positions. Additionally, removals must be considered at other critical locations as identified by engineering judgment. Such critical locations are typically associated with structural irregularities, which may include changes in plan geometry (e.g., re-entrant corners), discontinuities in vertical load paths (e.g., transfer girders), adjacent columns with significantly lower axial loads, variations in tributary areas, and changes in framing direction or elevation. Furthermore, if any other column is located within 30% of the largest bay dimension from a selected removal point, it must be removed simultaneously to capture potential interaction effects (Figure 7).

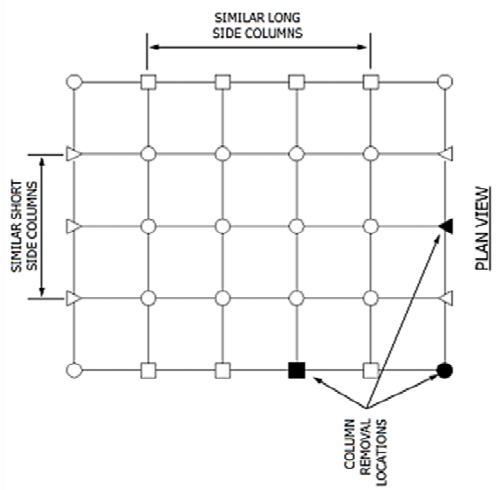

Figure 7. Location of external column removal (GSA, 2016)

In the context of progressive collapse assessment, the GSA provides a standardized approach for assigning load combinations to all structural components within the building being evaluated. The recommended loading conditions vary depending on the analytical method selected. Specifically:

- For Linear Static Analysis: The full Dead Load (DL) is applied, while Live Load (LL) is reduced to 25% of its nominal value.
- For Nonlinear Static and Nonlinear Dynamic Analyses: The full DL is used, and LL is taken either as 0% or 25%, depending on the design intent and occupancy assumptions.

The Dead Load (DL) is automatically computed by the analysis software based on the defined material properties, cross-sectional geometry, and gravity effects, ensuring consistency and minimizing user-based uncertainties.

In this study, the Live Load (LL) was conservatively assumed as 0%, in accordance with GSA recommendations for nonlinear dynamic analysis, assuming the building is unoccupied at the time of the initiating event.

2.2. Overview of the Applied Element Method (AEM)

The Applied Element Method (AEM) combines the strengths of the finite element method (FEM) with discrete modeling techniques. Since its introduction in 1995, AEM has been extensively developed and validated. Its fundamental concept is to represent a structure using small rigid elements, typically cubic, which are connected by normal (kn) and shear springs (ks) distributed over their surfaces. Each spring plays a distinct role in simulating structural behavior [26]. Normal springs handle axial forces, while shear springs are critical for capturing lateral deformations, including phenomena such as sliding, buckling, and crack propagation under extreme loads like earthquakes and blasts.

The stiffness of a normal spring is calculated using Equation 1:

$$k_n = \frac{E.\mathrm{A}}{d} \tag{1}$$

Here, E is the Young's modulus (resistance to axial deformation), A is the cross-sectional area of the spring (force capacity per unit deformation), and d is the distance between nodes (spatial configuration). Similarly, the stiffness of a shear spring is given by Equation 2:

$$k_s = \frac{G.A_s}{d} \tag{2}$$

where G is the shear modulus (resistance to shear deformation), As is the effective shear area (shear force transfer region), and d again represents the distance between connected nodes. This stiffness governs how elements respond to transverse forces and is vital for accurate simulation under dynamic or impact loading [27].

In contrast to FEM, where deformations are calculated inside elements, AEM concentrates deformations in the springs. This means that stress and strain values are primarily derived at spring locations. All individual spring stiffnesses are assembled into a global stiffness matrix K, which governs the system's overall behavior. The equation of motion is then solved through an implicit time integration method, assuming small displacements at each time step.

A distinctive feature of AEM is its ability to simulate fracture. When the cumulative strain in a spring exceeds a defined separation threshold, the spring connection breaks, and the elements act as independent rigid bodies. To handle contact between detached elements, a penalty-based contact algorithm is employed. This enables the transmission of compressive and shear forces during contact, allowing the method to capture phenomena like crack closure or impact rebound.

The stiffness matrix for a pair of springs is derived by considering their relative position (x, y, z) to the element centroid. This matrix expresses the relationship between forces and displacements at the connection and accounts for the material and geometric properties of the springs. A simplified version of this matrix is presented below as Equation 3, incorporating terms for both axial and shear contributions in all directions [28].

$$K = \begin{bmatrix} k_n & 0 & 0 & 0 & k_n z & -k_n y \\ 0 & k_s & 0 & -k_s z & 0 & k_s x \\ 0 & 0 & k_s & k_s y & -k_s x & 0 \\ 0 & -k_s z & k_s y & k_s(y^2+z^2) & -k_s xy & -k_s xz \\ k_n z & 0 & -k_s x & -k_s yx & k_n z^2 + k_s x^2 & -k_n yz \\ -k_n y & k_s x & 0 & -k_s zx & -k_n zy & k_n y^2 + k_s x^2 \end{bmatrix} \tag{3}$$

To compute the global matrix K, individual contributions from all springs are summed. Each spring affects certain degrees of freedom (DOFs)—including translational and rotational motions. For example, as illustrated in Equation 4, a single contact spring contributes one-quarter of its stiffness to the total matrix. The orientation and position of the spring (described by angles θ and α) influence how its stiffness components are projected into the global coordinate system [29].

$$\begin{bmatrix} \sin^2(\theta+\alpha)K_n & -K_n \sin(\theta+\alpha)\cos(\theta+\alpha) & K_s\, Lsin(\alpha)\, cos(\theta+\alpha) \\ +\cos^2(\theta+\alpha)K_s & +K_s\, sin(\theta+\alpha)\, cos(\theta+\alpha) & -sin(\theta+\alpha)\, K_n\, Lcos(\theta) \\ -K_n \sin(\theta+\alpha)\cos(\theta+\alpha) & \sin^2(\theta+\alpha)K_s & \cos(\theta+\alpha)K_n\, Lcos(\theta) \\ +K_s\, sin(\theta+\alpha)\, cos(\theta+\alpha) & +\cos^2(\theta+\alpha)K_n & +\sin(\theta+\alpha)\, K_s\, Lsin(\theta) \\ \cos(\theta+\alpha)K_s\, Lsin(\alpha) & \cos(\theta+\alpha)K_n\, Lcos(\alpha) & L^2\, cos^2(\alpha)K_n \\ -sin(\theta+\alpha)\, K_n\, Lcos(\alpha) & +\sin(\theta+\alpha)\, K_s\, Lsin(\theta) & +L^2\, sin^2(\alpha)K_s \end{bmatrix} \tag{4}$$

The matrix entries include terms involving Kn, Ks, and trigonometric expressions of θ+α, which represent the alignment of the spring with respect to the element. These mathematical components allow the AEM to simulate not only internal forces but also global deformations and failure mechanisms such as element separation, rotation, and collision.

In summary, the AEM provides a robust framework for modeling complex structural responses under extreme conditions. By combining element-based rigid body motion with spring-based deformation mechanics, it bridges the gap between continuum mechanics and discrete failure analysis, enabling realistic simulations of damage, fracture, and collapse (Figure 8).

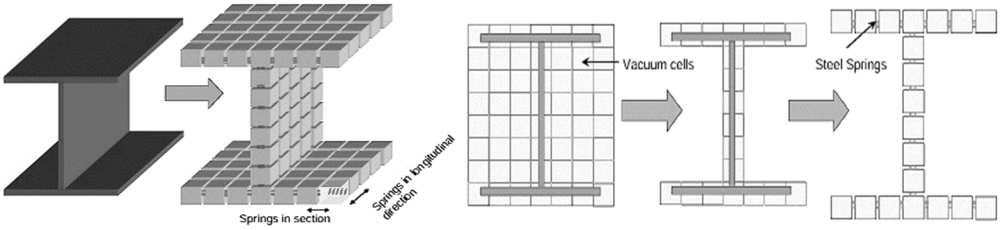

Figure 8. Applied element method steel elements with springs in section and longitudional direction

3. MAIN MODEL

The three-dimensional representation of the main structural model is shown in Figure 9a. The frame is composed of steel moment-resisting connections with rigid joints, designed to capture the global behavior under progressive collapse scenarios. The building consists of five stories with regularly spaced bays in both directions, as previously described. The zoomed-in view highlights the typical beam-to-column joint detailing, where beams from orthogonal directions converge at a shared column.

Figure 9a also presents detailed views of the beam-to-column connections. Each joint configuration includes beams from both longitudinal and transverse directions, connected to a central Wide Flange steel column. These rigid joints are modeled using full fixity assumptions, ensuring moment transfer between members. Additionally, the structural model uses ‘’I and wide flange ’’ sections for beams and columns to improve torsional rigidity and simplify mesh discretization for numerical simulations. The detailed mesh view confirms the continuity of members and the accuracy of element connectivity throughout the frame (Figure 9b).

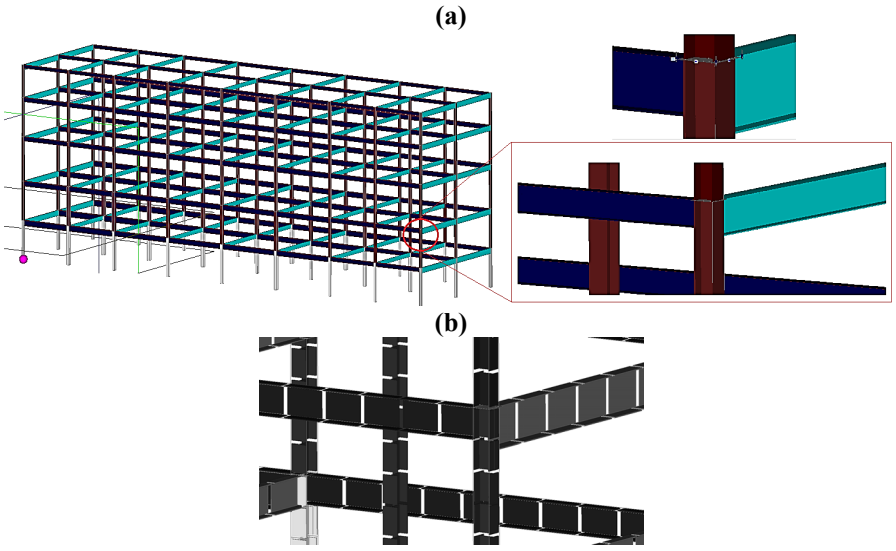

Figure 9. 3D Model rigid joints with wide flange sections (a) mesh view (b)

Table 3 summarizes the cross-sectional properties of the columns and beams used in the structural model. The table lists the member designations, their corresponding American steel section types, mass per unit

length (kg/m), and section depths (mm). Columns are labeled from A1 to A9 and beams from B1 to B9, following the grid system introduced earlier. The values are presented in SI units with approximate conversions where necessary. These specifications are crucial for accurately representing the structural behavior in the numerical analysis.

Table 3. Column and beam sections (SI units – approximate)

Column number	Column type (US)	Mass (kg/m)	Depth (mm)	Beam number	Beam type (US)	Mass (kg/m)	Depth (mm)
A1	10 WF 72	107.2	254	B1	24 B 76	~113.1	~610
A2	12 WF 133	198.0	305	B2	21 B 68	~101.2	~533
A3	12 WF 120	178.6	305	B3	16 B 58	~86.3	~406
A4	10 WF 100	148.8	254	B4	21 WF 62	92.3	533
A5	10 WF 89	132.5	254	B5	18 WF 50	74.4	457
A6	10 WF 54	80.4	254	B6	14 B 17.2	~25.6	~356
A7	10 WF 112	166.7	254	B7	14 B 22	~32.7	~356
A8	10 WF 60	89.3	254	B8	24 WF 76	113.1	610
A9	10 WF 33	49.1	254	B9	18 WF 45	66.9	457

The primary structural system considered in this study consists of a multi-bay steel moment-resisting frame. The plan view of the building, shown in Figure 10, includes seven spans in the longitudinal (X) direction and three bays in the transverse (Y) direction. The span lengths are not uniform; the outermost spans measure 6.50 meters, while the five intermediate spans are each 7.72 meters wide. This results in a total building length of approximately 51.38 meters in the X direction. Similarly, the transverse direction consists of three uniform bays, each 7.625 meters wide, totaling approximately 22.875 meters.

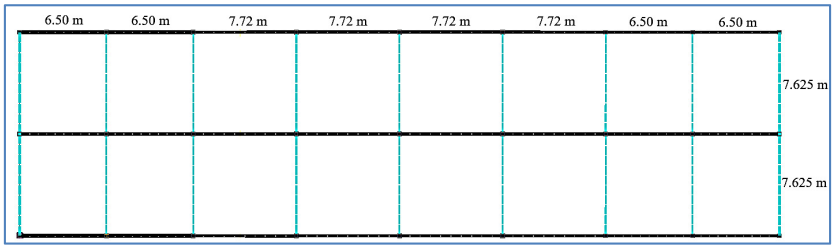

Figure 10. Plan view

The elevation view, illustrated in Figure 11, presents a five-story configuration with varying interstory heights. From the bottom to the top floor, the story heights are 4.45 m, 4.45 m, 5.06 m, 4.47 m, and 3.71 m, respectively, yielding a total building height of approximately 22.14 meters. Each floor is denoted with a grid system using both vertical (A1 to A9) and horizontal (B1 to B7) labeling to define beam and column locations for structural modeling and progressive collapse assessment (Table 3). The base level includes pinned conditions at the base columns (Figure 11).

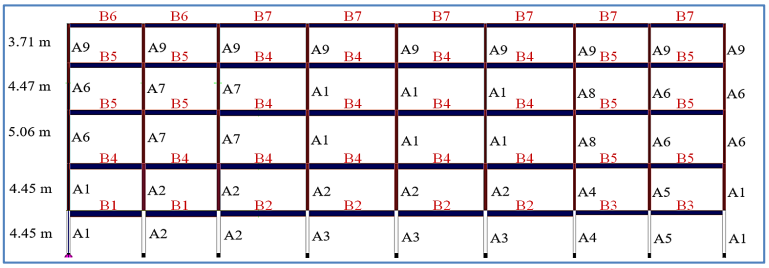

Figure 11. Elevation view of the five-story frame with varying interstory heights and grid labeling

The scenarios depicted in Figure 12 illustrate different potential outcomes of column removals, adapted from GSA (2016) guidelines. While GSA typically considers column removals one story above ground level, in this study, the columns are removed directly from the first story. This modification is based on observations from recent earthquakes in Türkiye, where significant damage, excessive displacements, or complete collapses have frequently occurred at the first-story columns.

Scenario (a) involves the removal of a corner column, which may compromise the stability of the building's perimeter, as corner columns are critical in maintaining boundary integrity. In scenario (b), the removal of an intermediate column on the long side could trigger a redistribution of loads along the structure's length, potentially overloading adjacent columns. Scenario (c) addresses the removal of an intermediate column on the short side, which might affect the lateral load distribution and influence the building's response to horizontal forces. These scenarios collectively aim to represent realistic collapse mechanisms by taking into account vulnerabilities observed in actual seismic events. In summary, according to GSA 2016, the model includes exterior column removal scenarios: (a) corner column, (b) intermediate column on the long side, and (c) intermediate column on the short side (Figure12).

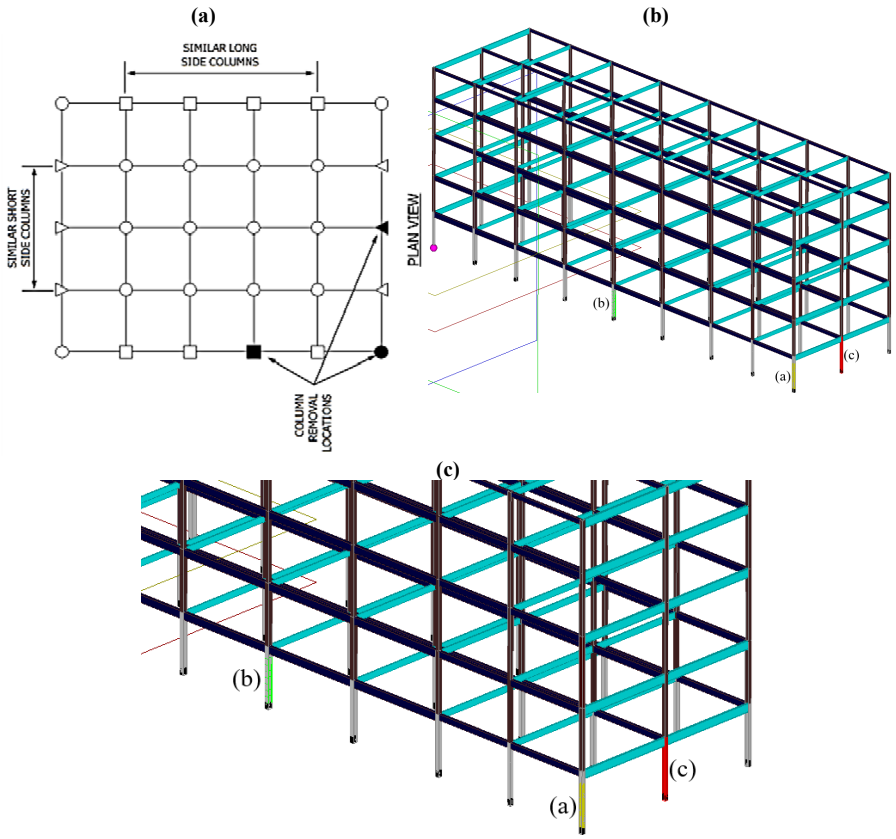

Figure 12. Column removal scenarios per GSA (2016) (a) model view (b) locations of removed columns (c)

The mechanical properties of the steel profiles used in this study are based on typical values for ASTM A992 Grade 50 steel, which is commonly employed for wide flange sections in structural applications. This steel grade has a minimum yield strength of 345 MPa, and a typical tensile strength of approximately 450–550 MPa. These properties are consistent across both the column and beam elements, and were used in the numerical analysis.

4. RESULTS

In this paper, the displacement response of the structure under different column removal scenarios was evaluated to investigate the progressive collapse potential. Figures 13-15 illustrate the time-history of vertical displacements for three different removal positions at the first story: corner column, middle of the long side, and middle of the short side.

This figure presents the structural response following the removal of a corner column. Subfigure (a) illustrates the location of the removed column, while subfigure (b) shows the corresponding graphical displacement results. A downward vertical displacements are observed near the removal zone, indicating a concentrated redistribution of loads toward adjacent members (Figure 13).

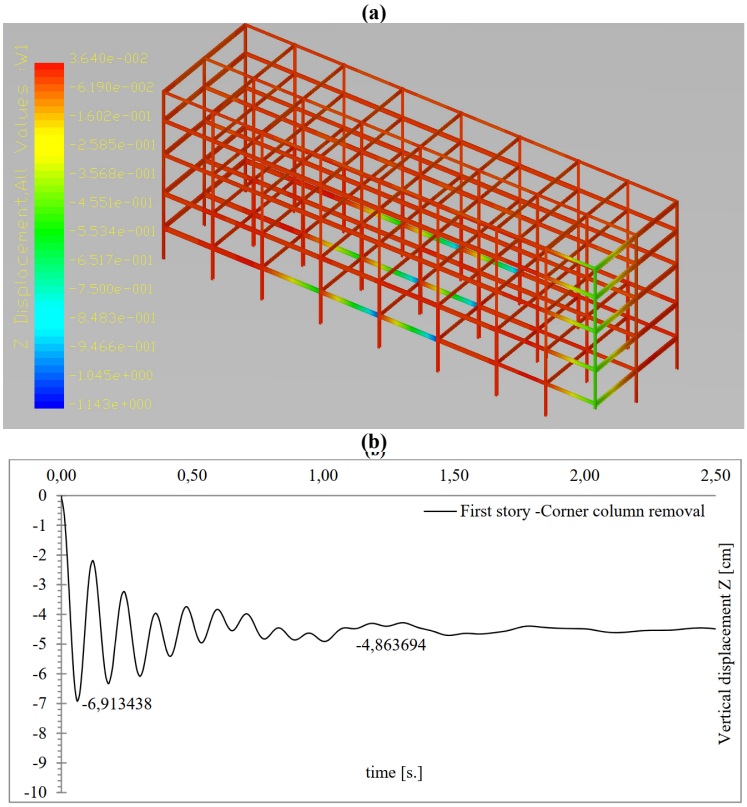

Figure 13. Corner column removal (a) and graphical displacement results (b)

Figure 14 below demonstrates the effects of removing an intermediate column located along the long side of the structure. Subfigure (a) identifies the removed column position, and subfigure (b) provides the displacement distribution. Compared to the corner removal scenario, a more pronounced displacement field extends along the longitudinal direction, suggesting a broader load transfer region.

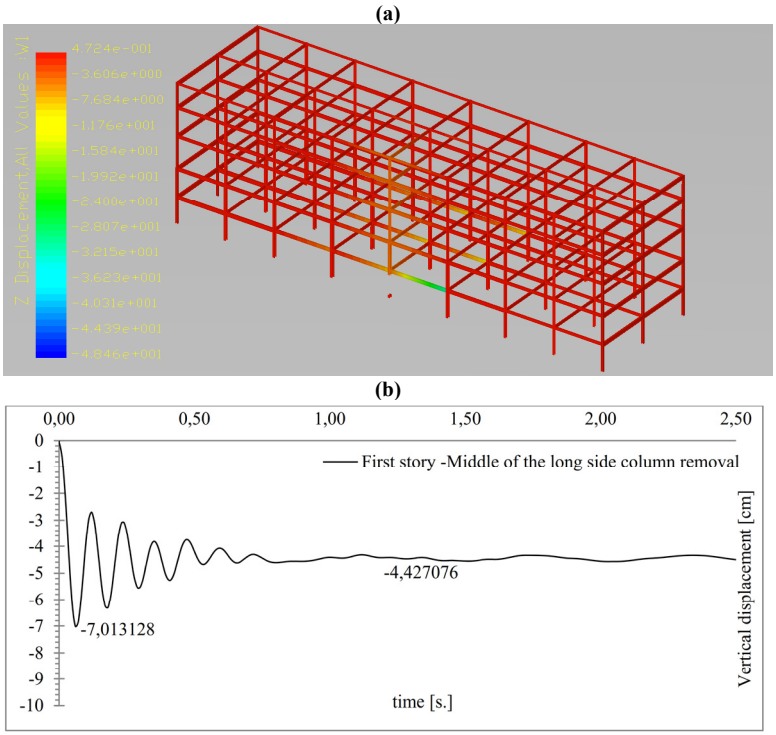

Figure 14. Removal of an intermediate column on the long side (a) and graphical displacement results (b)

A comparison of the vibration periods reveals that the removal of a corner column (Figure 13) leads to a relatively shorter vibration period compared to the other scenarios. The oscillations decay more rapidly, indicating a more localized redistribution of loads. In contrast, the removal of a middle column on the long side (Figure 14) results in the longest vibration period among the three cases. This behavior suggests a broader structural participation and a more extensive redistribution of loads along the longitudinal direction of the building. The removal of a middle column on the short side produces an intermediate response, with a vibration period slightly longer than that observed in the corner removal case but shorter than that of the long-side middle column removal (Figure 15).

This variation in vibration periods can be attributed to the structural configuration and the load-carrying mechanisms activated after column loss. Specifically, the long side of the building, having more structural redundancy and continuity, exhibits slower and more prolonged oscillations following column removal. On the other hand, the short side, offering less redundancy, shows a quicker stabilization, although still slower than the response observed after a corner column removal. Overall, the results highlight the importance of column location in the dynamic behavior of structures subjected to sudden column loss.

Figure 15 illustrates the response to the removal of an intermediate column situated on the short side of the building. Subfigure (a) pinpoints the removed column, while subfigure (b) displays the graphical displacement outcomes. Displacements are mainly localized near the short side, and the magnitude is slightly lower than those observed in the long side removal case.

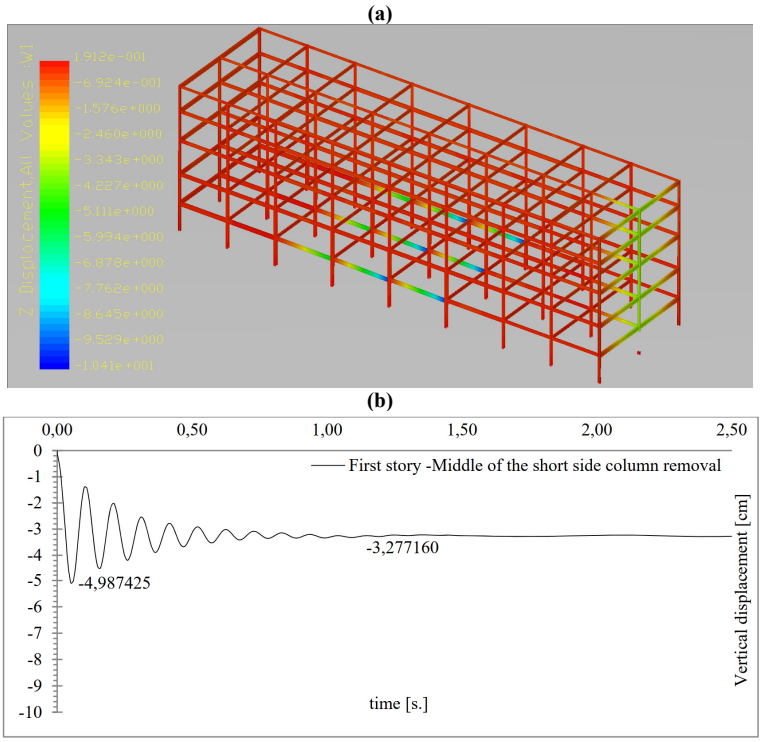

Figure 15. Removal of an intermediate column on the short side (a) and graphical displacement results (b)

Table 4 summarizes the maximum transient and residual vertical displacements recorded following the removal of different columns.

Table 4. Maximum transient and residual vertical displacements after the removal of columns

Column removal scenario	Max transient displacement(cm)	Residual displacement (cm)
Middle of the short side column	-4.99	-3.28
Middle of the long side column	-7.01	-4.43
Corner column	-6.91	-4.86

The results also show that the largest transient displacement occurred in the case of removing the middle column of the long side, reaching approximately -7.01 cm, followed closely by the corner column removal

at -6.91 cm. The middle column of the short side resulted in a relatively smaller peak transient displacement of -4.99 cm. This indicates that the location of the removed column significantly influences the dynamic response of the structure. Similarly, the residual displacements followed a consistent pattern. The middle of the long side removal again caused the most significant residual deformation (-4.43 cm), while the short side yielded the smallest (-3.28 cm). These findings highlight the vulnerability of the structure when columns are removed from the long-span bays or corner regions, due to increased load redistribution demands.

5. CONCLUSION

This study evaluated the progressive collapse behavior of a real five-story steel moment-resisting frame consist of non-uniform span lengths and varying story heights. It presents a numerical investigation into the progressive collapse of a five-story steel moment-resisting frame subjected to sudden column loss scenarios. Three column removal scenarios were analyzed to assess the system's vulnerability to progressive collapse: the middle column on the short side, the middle column on the long side, and a corner column. Utilizing the Applied Element Method, the study captured the global response of the structural system, including large-scale displacements and post-failure dynamics.

Among the scenarios evaluated, the removal of the central column along the long side induced the most critical response in terms of both peak and residual vertical displacements. In contrast, the short-side removal scenario exhibited comparatively lower displacement demands, demonstrating a localized and less severe impact on overall stability. Residual deformations across scenarios suggest that the location and surrounding bay geometry significantly influence both the extent and pattern of collapse propagation.

The analysis further confirms that longer spans and wider bay configurations, as seen in the longitudinal direction of the structure, may increase susceptibility to larger displacements following localized failure. These findings emphasize the importance of span proportion for further studies and column location in evaluating the collapse performance of steel frames and highlight the need for careful attention to geometric layout during design and robustness assessment.

Lastly, it is recommended to incorporate progressive collapse analysis alongside standard performance evaluations, as it enables the identification of critical weak points to prevent total collapse in the event of column loss, and strengthening of these points especially in case of earthquakes [30,31].

6. REFERENCES

1. Lu, J.X., Wu, H. & Fang, Q. (2022). Progressive collapse of Murrah Federal Building: Revisited. *Journal of Building Engineering, 57,* 104939.

2. Nist Ncstar, (2005). Final report on the collapse of the World Trade Center Towers. National Construction Safety Team for the Federal Building and Fire Safety Investigation of the World Trade Center Disaster. *National Institute of Standards and Technology,* Gaithersburg, MD.

3. Yu, J. & Tan, K.H. (2013). Experimental and numerical investigation on progressive collapse resistance of reinforced concrete beam column sub-assemblages. *Engineering Structures, 55,* 90-106.

4. Yuzbasi, J. (2024). Controlled demolition: novel monitoring and experimental validation of blast-induced full-scale existing high-rise building implosion using numerical finite element simulations. *Journal of Civil Structural Health Monitoring*, 1-24.

5. Shi, Y. & Jiang, R. (2024). Experimental investigation on progressive collapse performance of RC substructures under blast loading. *Structures, 70,* 107803.

6. Ellingwood, B.R., Smilowitz, R., Dusenberry, D.O., Duthinh, D., Lew, H.S. & Carino, N.J. (2007). Best practices for reducing the potential for progressive collapse in buildings. *National Institute of Standards and Technology,* Gaithersburg, 216.

7. Ellingwood, B.R. (2006). Mitigating risk from abnormal loads and progressive collapse. *Journal of Performance of Constructed Facilities, 20*(4), 315-323.

8. Yuzbasi, J. (2024). Experimental verification of full-scale silo structure demolition: Investigating successive column removal with finite element method and progressive collapse simulation through blast load. *Structural Concrete*, *25*(6), 4408-4427.

9. Avcil, F., Işık, E., İzol, R., Büyüksaraç, A., Arkan, E., Arslan, M.H., Aksouylu, C., Eyisüren, O. & Harirchian, E. (2024). Effects of the February 6, 2023, Kahramanmaraş earthquake on structures in Kahramanmaraş city. *Natural Hazards, 120*(3), 2953-2991.

10. Işık, E., Hadzima-Nyarko, M., Avcil, F., Büyüksaraç, A., Arkan, E., Alkan, H. & Harirchian, E. (2024). Comparison of seismic and structural parameters of settlements in the East Anatolian fault zone in light of the 6 February Kahramanmaraş earthquakes. *Infrastructures*, *9*(12), 219.

11. Yuzbasi, J. (2024). Post-earthquake damage assessment: field observations and recent developments with recommendations from the Kahramanmaraş earthquakes in Türkiye on February 6th, 2023 (Pazarcık M7. 8 and Elbistan M7. 6). *Journal of Earthquake Engineering,* 1-26.

12. Alashker, Y., El-Tawil, S. & Orsi, G. (2011). Improving the progressive collapse resistance of steel moment frames using FRP. *Journal of Constructional Steel Research, 67*(3), 401-413.

13. Bao, Y. & Yang, B. (2012). Energy flow in progressive collapse of steel-framed buildings. Engineering Structures, 42, 142-153.

14. Bregoli, D., Lagaros, N.D. & Limongelli, M.P. (2017). Structural robustness of steel-framed modular buildings using the alternative load path method. *Engineering Structures, 151,* 488-502.

15. Lu, X., Lin, K., Guan, H. & Ye, L. (2005). Progressive collapse resistance of high-rise steel moment frames designed for earthquakes. *In Proceedings of the 2005 ASCE Structures Congress*, 1-10.

16. Li, Y., Song, R. & Van De Lindt, J.W. (2014). Collapse fragility of steel structures subjected to earthquake mainshock-aftershock sequences. *Journal of Structural Engineering*, *140*(12), 04014095.

17. Stochino, F., Bedon, C., Sagaseta, J. & Honfi, D. (2019). Robustness and resilience of structures under extreme loads. *Advances in Civil Engineering, 2019*(1), 4291703.

18. Işık, E., Peker, F. & Büyüksaraç, A. (2022). The effect of vertical earthquake motion on steel structures behaviour in different seismic zones. *Journal of Advanced Research in Natural and Applied Sciences*, *8*(3), 527-542.

19. Domaneschi, M., Pellechia, C., De. Iuliis, E., Cimellaro, G.P., Morgese, M., Khalil, A.A. & Ansari, F. (2020): Collapse analysis of the Polcevera viaduct by the applied element method. *Engineering Structures, 214,* 110659.

20. Yuzbasi, J. & Arslan, H.M. (2025). Applied element method and Finite element method for progressive collapse assessment: A comparative study on the influence of slab types, thicknesses, and damping via three incremental column removals. *Structures, 73,* 108358).

21. Extreme Loading® for Structures V9 ELS Theoretical Manual, (2022). https://www.extreme loading.com/wp-content/uploads/els-v9-theoretical-manual.pdf

22. Song, B.I. (2010). Experimental and analytical assessment on the progressive collapse potential of existing buildings. *Master's thesis.* The Ohio State University.

23. General Services Administration, (2016). *Alternate path analysis & design guidelines for progressive collapse resistance* (Revision 1). Washington, DC: U.S. General Services Administration.

24. American Society of Civil Engineers, (2017). *Seismic evaluation and retrofit of existing buildings* (ASCE/SEI 41-17). Reston, VA: American Society of Civil Engineers.

25. U.S. Department of Defense, (2009). *Design of buildings to resist progressive collapse* (UFC 4-023-03, Change 4, 10 June 2024). Washington, DC: U.S. Department of Defense.

26. Meguro, K. & Tagel-Din, H. (2001). Applied element method: A new efficient tool for design of structure considering its failure behavior. *Institution of Industrial Science (IIS)*, 1-20. The University of Tokyo.

27. Meguro, K. & Tagel-Din, H. (2000). Applied element method for structural analysis theory and application for linear materials. *Doboku Gakkai Ronbunshu, 2000*(647), 31-45.

28. Meguro, K. & Tagel-Din, H. (2001). Applied element simulation of RC structures under cyclic loading. *Journal of Structural Engineering, 127*(11), 1295-1305.

29. Tagel-Din, H. & Meguro, K. (2000). Applied element method for dynamic large deformation analysis of structures. *Doboku Gakkai Ronbunshu, 2000*(661), 1-10.

30. Yüzbaşı, J., & Yerli, H.R. (2018). Betonarme yapıların deprem etkisi altında performans analizlerinin yapılması ve güçlendirilmesi. *Çukurova Üniversitesi Mühendislik-Mimarlık Fakültesi Dergisi*, *33*(2), 273-286.

31. Akıncı, A.C. & Ünlügenç, U.C. (2023). 6 Şubat 2023 Kahramanmaraş depremleri: sahadan jeolojik veriler, değerlendirme ve Adana için etkileri. *Çukurova Üniversitesi Mühendislik Fakültesi Dergisi*, *38*(2), 553-569.